Initial stages of nickel oxide growth on Ag(001) by pulsed laser deposition

S. H. Phark,[*] Young Jun Chang, and T. W. Noh

ReCOE and FPRD, Department of Physics and Astronomy, Seoul National University, Seoul 151-747, Korea

J.-S. Kim[†]

Department of Physics, Sook-Myung Women's University, Seoul 140-742, Korea

Submonolayers of nickel oxide films were grown on an Ag(001) by pulsed laser deposition, and characterized *in situ* by both scanning tunneling microscopy and x-ray photoelectron spectroscopy. We observed quasi-two-dimensional growth of the film, and clearly identified several kinds of defects, such as embedded metallic Ni clusters and, notably, oxygen atoms, even while looking deeply into the substrate. These originated from Ni and O hyperthermal projectiles as well as from NiO clusters that were formed during laser ablation of a NiO target. Those defects played a role of nucleation sites in extending the nucleation stage of thin-film growth.

I. INTRODUCTION

Metal-oxide heterostructures have played essential role in numerous applications, and have been used as heterogeneous catalysts, magnetic tunnel junction, and resistance change random access memory.[1,2] They have also revealed interesting physical phenomena ranging from quantum confinement effects[3] to tunneling effects[4,5] to exchange bias.[6] These intriguing properties are quite sensitive to even monolayer-scale details in their atomic and chemical structures at the interface.[3,5,7–10] The growth of well-defined interfaces and their characterization at the atomic scale is therefore an important issue in the study of metal-oxide heterostructures.

To grow oxide layers on metallic substrates, various forms of thermal vapor deposition under ambient oxygen environments have been used. However, since the pulsed layer deposition (PLD) accompanies hyperthermal deposits, it gives rise to growth modes and structures of thin films that the conventional thermal evaporation does not allow. For example, the ferromagnetic thin films grown by PLD showed different growth modes and magnetic properties from those grown by thermal evaporation.[11] Besides, for the growth of oxide superlattices, PLD is the widely accepted standard technique due to its excellent performance in producing high-quality crystalline films with precise thickness control down to the atomic regime.[12] This strongly suggests, investigating, whether PLD could also produce high-quality oxide layers on metallic substrates, and, further, how the energetic deposits formed during PLD would affect the growth kinetics of these oxide films.

These studies may also offer information on the interface structure formed during sputter deposition, an industrial standard in which similar energetic deposits are incident, but the interface structure is not much investigated due to rough polycrystalline structures of the oxide films. Recently, polycrystalline NiO films attract great interests in the field of solid-state electronic devices such as resistive random access memory.[13] A critical disadvantage of NiO is poor switching endurance, and the origin of this unstable switching behavior was frequently attributed to the defective phases at the metal-oxide interfaces.[14,15]

Since Ag(001) is a near ideal substrate for NiO epitaxy due to its low reactivity and small lattice mismatch (~2% compressive), several researchers have investigated ultrathin NiO films grown on Ag(001) substrates as a model oxide-metal heterostructure. Moreover, NiO is an interesting material with intriguing electronic properties as a charge transfer insulator with antiferromagnetic order, and its applications in catalysis[16,17] and magnetic nanodevices.[18]

The structure and morphology of NiO films on Ag(001) have been investigated using numerous probes, including low-energy electron diffraction (LEED), auger and photoelectron diffraction,[19–21] scanning tunneling microscopy (STM),[22,23] spot profile analysis LEED,[24] primary-beam diffraction-modulated electron emission,[25] and specular x-ray reflectivity.[26] These studies in the submonolayer regime found a $p(2 \times 1)$ phase plus chemical defects such as metallic Ni and nonstoichiometric Ni oxides at the very interface. From the second layer, however, NiO films were found to grow in a layer-by-layer fashion on Ag(001) in a pseudomorphic, tetragonally distorted rocksalt phase.

In this work, we performed *in situ* STM and x-ray photoelectron spectroscopy (XPS) studies on nickel oxide films grown on Ag(001) by PLD. It was revealed that nickel oxide films grow in a quasi-layer-by-layer fashion. Numerous irregular defect structures, originated from the neutral Ni and O atoms, were also found on the surface of the substrate. It seemed that the nucleation stage was much elongated due to the high density of those surface defects. In addition, we obtained direct evidence for the existence of hyperthermal oxygen atoms, diffused during PLD, to the depth of $\sim \mu$m below the substrate surface.

II. EXPERIMENT

All the experiments were carried out in a multichamber system combining an ultrahigh vacuum (UHV) PLD chamber and a UHV characterization chamber. The PLD chamber maintained a base pressure of $<2 \times 10^{-9}$ Torr, and was equipped with a reflection high-energy electron diffractometer. The characterization chamber maintained a base pressure of $<2 \times 10^{-10}$ Torr, and was equipped with STM and XPS. This system makes *in situ* sample preparation and characterization possible.
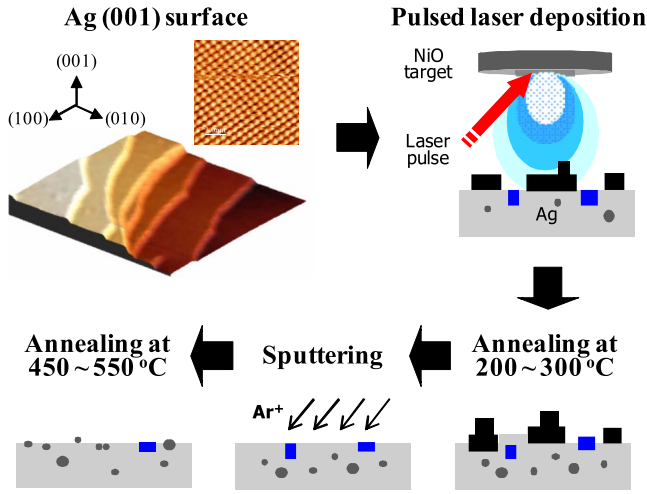
FIG. 1. (Color online) Schematic of the experimental procedure. Submonolayer films of nickel oxide were grown on an Ag(001) surface by using the PLD technique. Black rectangles, blue (gray) rectangles, and dark gray circles denote the islands or clusters formed on the surface, at the subsurface, and deep inside the substrate, respectively. Annealing as-grown films at 200–300 °C in UHV, make the monolayer nickel oxide islands more three-dimensional like, and formed metallic clusters of several nm widths in the surface and subsurface layers. Removing the oxide islands by the Ar$^+$ sputtering followed by 450–550 °C postannealing forced the defects deep inside the substrate to move to the near-surface region. *In situ* STM and XPS measurements were performed on each experimental step.

We prepared a clean Ag(001) single crystalline substrate by repeated cycles of Ar$^+$ sputtering and annealing at 450 °C for 30 min. The STM image of a typical Ag(001) surface in Fig. 1 shows atomically flat terraces of several hundred nanometers, separated by monotonically high steps. As shown in the inset of Fig. 1, the crystalline orientation is identifiable from an atomic resolution STM image. For all the STM experiments, we used electrochemically etched tungsten tips and applied a bias voltage to the sample (V_{sample}) while the tip was grounded. For the nickel oxide film deposition, a KrF excimer laser ($\lambda = 248$ nm) with a repetition rate of 1 Hz was used. The target was sintered polycrystalline NiO, and the energy density was about 3 J/cm^2 at the target surface. During deposition, the oxygen partial pressure (P_{O2}) was 1 $\times 10^{-6}$ Torr and the sample stage was maintained at room temperature (RT).

Figure 1 is a schematic of the experimental procedures. We initially grew submonolayer nickel oxide films, which were then investigated by the STM. We used XPS to check the chemical states of the as-grown films. To observe how the surface structures and the chemical states changed with respect to temperature, we performed similar STM/XPS studies after annealing the 0.5 ML film at 200 and 300 °C for 10 min each in UHV. To further examine the subsurface defects, we performed similar STM/XPS studies after sputtering the nickel oxide film at RT with Ar$^+$ ions and then annealing at 450–550 °C. We repeated the Ar$^+$ sputtering and annealing experiments several times and investigated how the subsurface defects evolved with the sputtering/annealing cycles.
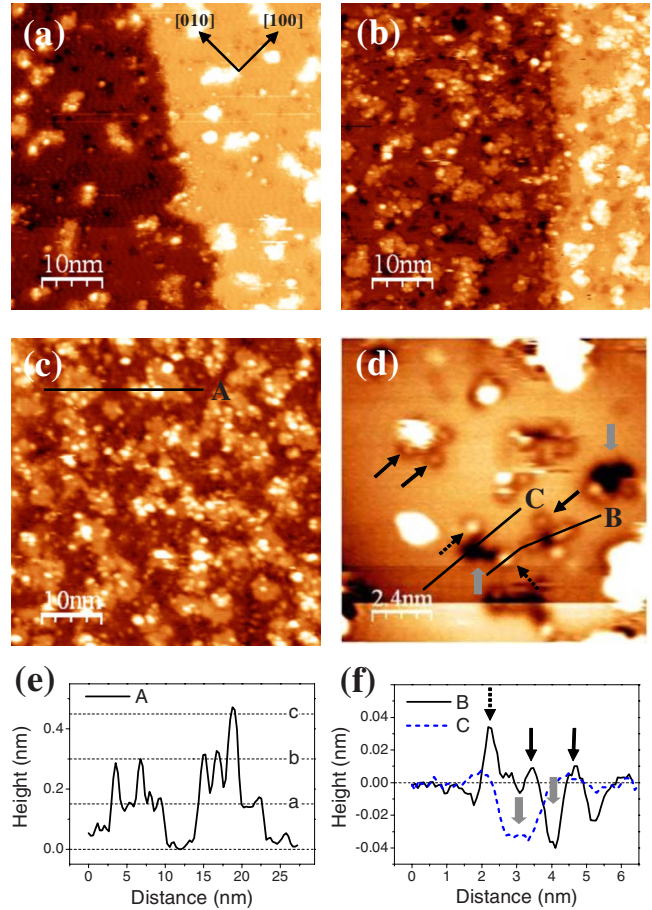

FIG. 2. (Color online) STM images obtained with V_{sample} =2.7 V from (a) 0.1, (b) 0.3, and (c) 0.5 ML nickel oxides grown on Ag(001) single crystal. (d) High-resolution STM image obtained from the 0.1 ML film. (e) Height profile along the line A. (f) Height profiles along the lines B and C in (d). (For each image, corresponding image size is denoted by the scale bar at the bottom-left corner.)

III. RESULTS AND DISCUSSION

A. As-grown films

1. Nickel oxide growth behavior at RT

Figures 2(a)–2(c) show the structural evolution of the as-grown film with increasing coverage (Θ). Figure 2(a) shows an STM image for $\Theta \sim 0.1$, which contained large islands. (As will be discussed in detail in Sec. III A 2, this surface also had various kinds of small surface species and defects.) Since we could obtain stable STM junctions showing realistic topographic images of the islands only at high (>1.5 V) bias voltages, we assigned these large islands to nickel oxide. All of the islands showed a nominal height of 0.15 nm, suggesting that they were of the same species. Among the surface diffusion processes of the deposits, it is much easier for them to move along the island edges since such motion requires the least breakage of bonds. However, as shown in Fig. 2(a), the edges of these islands were not straight but rather irregularly shaped. This indicates that diffusion should be quite limited, even along the edges of the islands.

Figure 2(b) shows an STM image for $\Theta \sim 0.3$. The mean size of the islands did not increase significantly, and coalescence of the islands was rarely observed. The morphological change came instead from the incrementing of the densities of both the islands and the defects. Note that the nucleation stage in the PLD-grown nickel oxide film was considerably more extended than those in the nickel oxide films grown by electron-beam evaporation (EBE).[22,23] This is also consistent with inefficient diffusion of the deposits on the terrace, as anticipated from the limited edge diffusion found in Fig. 2(a). This restricted diffusion should increase the density of ad species on the terraces during deposition and enhance the nucleation probability, thereby significantly extending the nucleation stage in the nickel oxide film growth.

Figure 2(c) shows an STM image for $\Theta \sim 0.5$ indicating coalescence of the large islands, with Fig. 2(e) showing the height profile along line A. Most islands were 0.15 nm high, as denoted by the dotted line "a." We also found bilayered and trilayered structures denoted by the dotted lines "b" and "c," respectively. However, the overall growth of the nickel oxide islands seemed to have two-dimensional (2D) characteristics. Similar 2D growth modes were reported for sub-monolayer nickel oxide films grown using EBE.[22,23]

2. Surface defects

Figure 2(d) shows a high-resolution STM image for $\Theta \sim 0.1$. In addition to the oxide islands, which appear as large white features, one can clearly observe depressed regions and a couple of adatomlike structures in the terrace, which are denoted by gray arrows and solid/dotted arrows, respectively. Figure 2(f) gives the height profile along lines B and C in Fig. 2(d), and indicates the topographic information across these defect structures.

The depressed regions (with the black contrast) in Fig. 2(f) were lower than the substrate surface by only ~ 0.04 nm, and their typical lateral size was on the order of 1 nm. Because these depressed regions were imaged nearly independent of the applied bias voltage, they should be metallic. Since the Ni atomic radius was 0.02 nm smaller than that of Ag, its center could be positioned lower than the original lattice site if it is incorporated in the surface layer of the Ag substrate. Thus, the Ni atom should appear as a more than 0.02-nm-deep depression in the Ag surface. Note that similar depressions in the STM contrast were observed when submonolayer Co films were grown on Ag(001) at RT using a low-energy (5–30 eV) ion deposition technique,[27] and that they were attributed to Co clusters in the surface layer of the Ag(001). Similarly, relatively small atomic radius of Ni and resultant low atomic position in the Ag lattice may cause the depression in the STM image while maintaining the metallic character of those regions. Therefore, it is highly probable that the depressed regions in Fig. 2(d) are metallic Ni clusters confined in the Ag(001) surface layer.

Oxide layer embedded in the Ag surface is another possible candidate for the origin of such depressions because STM data cannot be taken as the direct evidence to tell the chemical species forming the depressed regions. However, we exclude the possibility for the latter case with the following ground: we observed such depression in a NiO film grown on Ag(001) via reactive oxidation of thermally evaporated Ni.[28] They disappeared with increasing P_{O2}. Increased oxidation probability of Ni due to increased P_{O2} means the decrease in atomic Ni deposits which is easily incorporated into Ag substrate.

It has been known that ionic species are ordinarily produced during the laser ablation process.[29] Deposits ablated from the targets such as GaP,[30] $Bi_2Sr_2CaCu_2O_8$,[31] and $YBaCuO_7$ (Ref. 32) during PLD were investigated by the time-of-flight mass spectroscopy and the time-resolved high-resolution emission spectroscopy. They observed that numerous atomic/molecular compositions and ions of different charge states are generated, and that the energy distribution of them ranges from 1 to 10 eV with the laser fluence of $0.1-4$ J/cm^2. For NiO target, it is expected that the intense laser beam dissociates a large fraction of NiO into atomic/ionic Ni and O.[29]

If those Ni atomic/ionic deposits are not fully reoxidized during flight and after deposited on the substrate, they may dissolve into it to minimize the surface free energy. Bulk Ni-Ag system is well known to be immiscible, and undergoes a phase separation.[33] Besides, our earlier Monte Carlo simulations predicted that intermixing of Ni in the form of clusters at and below the Ag surface was energetically favored to reduce the surface free energy.[34] Those intermixing behaviors have been observed during the initial stages of Ni film growth using several different deposition techniques.[35,36] The bulk Rh-Ag system, which shows similar immiscible behavior for bulk, shows subsurface clustering of Rh deposited on Ag(001).[37] Therefore, although we used a NiO target, Ni atoms and ions produced during laser ablation in the PLD process form Ni clusters in the near surface of the Ag substrate, and are imaged as depressed regions by STM.

We next investigated the adatomlike structures shown in Fig. 2(d). We called the ball-shaped structures, indicated by solid arrows in both Figs. 2(d) and 2(f), Type-1 defects. These appeared slightly higher than the substrate surface, and were always surrounded by ring-shaped depressed regions, the so-called "sombrero" shape. Another type of defects, called Type-2, which are denoted by dotted arrows in both Figs. 2(d) and 2(f), were also ball shaped, but without any surrounding depression. Note that Type-2 defects appeared to be 0.02 nm higher than Type-1 defects.

Considering their circular shapes, small (~ 0.5 nm) diameters, and uniform sizes, we assigned both Type-1 and Type-2 defects to individual adatoms. There are interesting reports that a dosing of O_2 on Ag(001) at T=120–140 K could result in the dissociative adsorption of oxygen atoms on two different sites:[38,39] at a fourfold hollow and at an on-top site, giving rise to sombrero and "simple circular" STM images, respectively. As they are quite similar to STM images of our Type-1 and Type-2 defects, we assigned the Type-1 and Type-2 defects to oxygen atoms adsorbed onto fourfold hollows and on-top sites of Ag(001), respectively.

The question of how the oxygen atoms can dissociatively adsorb onto Ag(001) during the deposition at room temperature. The atomic/ionic oxygen formed by the laser ablation of the NiO target should be a source for the ball-shaped species. There seems to be another source. Note that all the ball-

shaped defects in Fig. 2(d) could be observed only around the rims of the nickel oxide islands (i.e., the large white regions) or the Ni clusters (i.e., the depressed regions). These observations suggest that those defect sites could be very reactive due to the low coordination and strain, and might effectively produce atomic oxygen via dissociation of ambient oxygen molecules as well as offer them the adsorption sites. Vattuone *et al.*[40] reported that defects on sputtered Ag(001) strongly enhance the dissociation probability of oxygen molecules, even at 105 K.

3. Relationship between surface defects and growth kinetics at RT

The RT growth pattern depicted in Fig. 2 can be summarized by a fairly extended nucleation stage when $\Theta < 0.5$, followed by the coalescence stage of the nickel oxide islands around ~0.5. Surface defects can play important roles in the extended nucleation process. In Figs. 2(a) and 2(b), the increase in island density was always accompanied by an increase in defects, especially in the depressed areas and the embedded Ni clusters. On the other hand, the island density rarely increased in Fig. 2(c), and coalescence proceeded instead.

Geometric defects are energetically unstable due to reduced coordination, and they could behave as nucleation sites. In the present case, chemical defects such as subsurface Ni can also offer extra nucleation channels. It has been reported that during the growth of Co films on Cu(001) and Ag(001), the embedded Co clusters act as nucleation sites for the growth of the overlying Co islands.[27] If such defects are constantly generated during deposition, the nucleation of new islands continues, and the growth of the pre-existing islands will be limited till the coalescence of islands occurs around 0.5 ML. Additionally, defects may limit the effective diffusion length due to strain fields around them and thus the growth of islands while increasing the chance for the formation of new islands within the otherwise island-free region.

B. Annealing effects on the nickel oxide films

1. Morphological changes

To understand the kinetics of the deposits on the surface, we postannealed the 0.5-ML-thick as-grown nickel oxide film at 200 and 300 °C for 10 min. Figure 3(a) shows an STM topographic image of the nickel oxide film after the 200 °C postannealing. With this thermal treatment, the average size of the oxide islands increased by ~20% (from ~49 nm^2 in the as-grown film to ~58 nm^2 in the annealed one). Relatively small (<5 nm^2) islands seemed to disappear, and the island edges became more straightened.[41] In spite of such changes, the overall morphological differences between the as-grown and the 200 °C postannealed films appeared to be minor. On the other hand, when the sample was postannealed at 300 °C, it experienced dramatic morphological changes, as shown in Fig. 3(b), where the area covered by the nickel oxide islands was significantly reduced. This leads to the conclusion that postannealing at a temperature greater than 200 °C is required to induce sig-
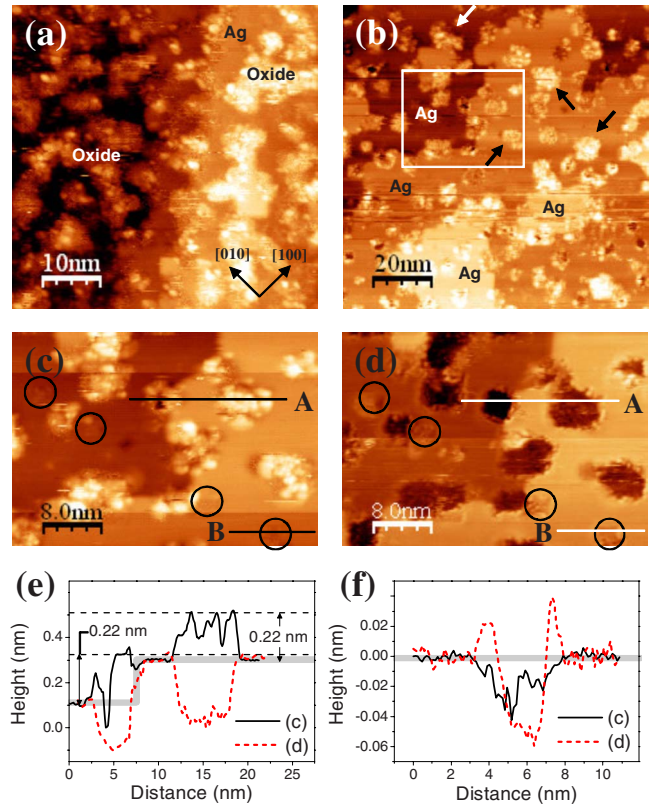

FIG. 3. (Color online) STM images of UHV-annealed 0.5 ML films at (a) 200 and (b) 300 °C. The arrows in (b) indicate oxide islands. For the boxed region in (b), higher resolution images were obtained with V_{sample} of (c) 2.5 and (d) 1.5 V. Height profiles were measured along the lines A and B in (c) and (d), and are shown for oxide islands and metallic Ni clusters in (e) and (f), respectively. The thick gray lines in the height profiles indicate the height of the Ag terraces.

nificant morphological changes in the as-grown film.

To obtain further insights into the morphological changes, we performed high-resolution STM measurements on the region marked by the black rectangular box in Fig. 3(b). Figures 3(c) and 3(d) show images of the same region, obtained with V_{sample} of 2.5 and 1.5 V, respectively. One can easily recognize the contrast reversal of the oxide islands between the images. By varying V_{sample}, we found that the contrast reversal took place abruptly at a V_{sample} of ~1.8 V.[42] This indicates that the conduction band of the oxide islands starts around 1.8 eV above the Fermi energy, E_F.[43,44] The solid black curve in Fig. 3(e) shows the height profiles along line A in Fig. 3(c), taken at V_{sample}=2.5 V. The apparent height of the oxide islands was 0.22 nm. Note that, as shown in Fig. 2(e), the height for a single nickel oxide layer in an STM image taken with V_{sample}=2.7 eV was estimated at about 0.15 nm. Since the STM should measure the apparent topographic height, the measured height for the insulating island was somewhat lower with V_{sample}=2.5 eV than with 2.7 eV.

Ultrathin films of MgO/Ag(001) deposited at 500 K (Ref. 45) and NiO/Ag(001) postannealed at 400−450 K (Ref. 46) showed the surface/subsurface incorporation of oxide islands into Ag substrates. For both cases, the oxides islands could be imaged as protrusions only at high V_{sample}, which indi-
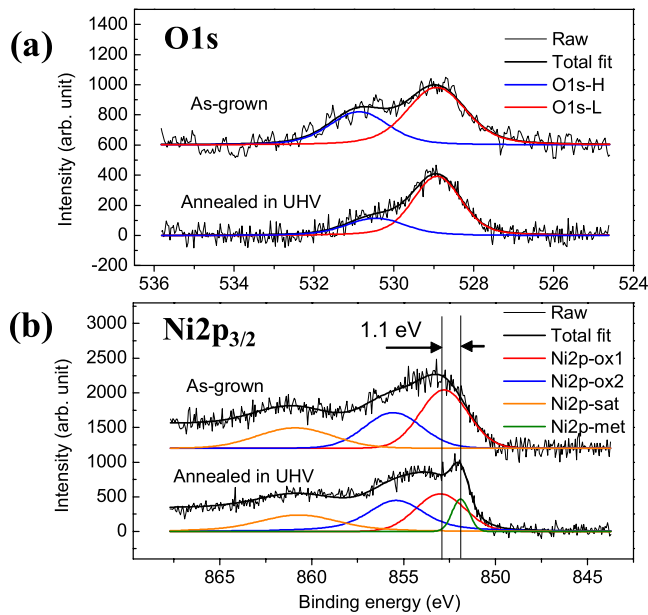
FIG. 4. (Color online) (a) O 1s and (b) Ni 2$p_{3/2}$ core level XPS spectra of the 0.5 ML film as-grown and annealed at 300 °C. For each spectrum, the black solid curve indicates the best fit to the experimental spectrum, and the red, blue, and orange curves are the fit curves of the individual charge valence states after the Shirley-type background subtraction.

cates the insulating nature of those islands. Großer et al.[46] observed that the STM of 3-ML-thick NiO islands undergoes contrast reversal between two images obtained at V_{sample} =2.5 and 1 V. They also observed that 2-ML-thick NiO islands show contrast reversal between two V_{sample}'s, although the contrast change is much less than those shown from the 3-ML-thick NiO islands.

STM topographic contrast cannot reveal the thickness of the oxide island. However, our observation of contrast reversal in Fig. 3 at V_{sample}=1.8 V is highly consistent with the Großer et al.'s results, although the specific tunneling conditions such as tip geometry can give a little effect on the contrast level. This suggests that the present islands have well-defined, large band gap, indicating that the thickness of NiO film is larger than 2 ML. This indicates to the possibility of the some NiO layer(s) embedded in Ag substrate, as also reported by many groups.[22,23,46] Therefore, we propose that the regions of 0.22 nm height in Fig. 3(e) should be the NiO layers thicker than 2 ML.

We also obtained O 1s core-level XPS spectra on both the as-grown and 300 °C annealed films. Figure 4(a) shows O 1s spectra for both cases. Each spectrum was fitted with two peaks, which we named by "O 1s-L" (with binding energy, E_b, of 529.2 eV) and "O 1s-H" (with E_b of 531 eV). The O 1s-L peak is due to the photoelectrons emitted from O^{2-} ions of stoichiometric NiO, but the origin of the O 1s-H peak is still controversial.[47–50] This peak can be attributed to oxygen ions in Ni_2O_3 compound,[50] in hydroxide [$Ni(OH)_2$],[47,49] or the adsorbed oxygen.[48] Despite the uncertainty about the origin of the second peak, it is quite clear that the decrease of the O 1s-H peak for the annealed sample indicates that the electronic structures of our nickel oxide

film became more bulklike from the thermal treatment. This change in O 1s XPS spectra is also consistent with multiple stacking of the nickel oxide layers.

2. Appearance of metallic Ni clusters in the Ag substrate

Besides the oxide islands, one can observe other features marked by circles in Figs. 3(c) and 3(d). As shown in Fig. 3(f), the topographic heights were nearly bias independent compared to those of the oxide islands, as is commonly observed in metallic systems. Further, they always appeared as depressions lower than the substrate surface by ~0.04 nm. Note that such a depression is quite similar to those observed in the STM image of as-grown films, i.e., Fig. 2(d). Due to this similarity, we also assigned the regions of the solid circles in Fig. 3 to embedded Ni clusters in the Ag substrate.[34–36]

We obtained Ni 2p core-level XPS spectra to verify this Ni cluster assignment. Figure 4(b) shows Ni 2$p_{3/2}$ spectra for both the as-grown and annealed samples. Following previous studies,[47–50] the Ni 2$p_{3/2}$ spectrum of the as-grown film was fitted with three peaks. A new peak appeared in the Ni 2$p_{3/2}$ spectrum of 300 °C annealed film at an E_b lower by 1.1 eV than that of nickel oxide. This new peak should originate from the neutral Ni species,[48,49] supporting our claim that metallic Ni clusters should be formed in the surface layer of a thermally treated Ag substrate.

C. Subsurface defects

The projectiles formed by the pulsed laser beam are incident on the substrate with a much higher kinetic energy than that of thermally evaporated species, and can therefore penetrate the substrate and form subsurface defects. We examined that possibility by unearthing them using sputtering and annealing processes.

To this end, we sputtered the nickel oxide film, which had been postannealed at 300 °C, as discussed in Sec. III B, for 60 min. We then annealed it at 450 °C for 60 min. Figure 5(a) shows the Ag(001) surface after having undergone the above cleaning processes. Most of the oxide islands were removed from the surface, but some ball-shaped structures, with a mean diameter of less than 0.4 nm, could still be observed. As annealing temperature was increased to 550 °C, their population increased monotonically, as shown in Figs. 5(b) and 5(c). Their population also multiplied with an increase in annealing time (figure not shown), implying that annealing forced the defects to float from the subsurface to the near-surface region. These particles were observed in STM images even after 3 additional hours of sputtering followed by 450 °C annealing.[51] Because of the difficulty of any atomic/ionic species residing near a surface surviving under such harsh sputtering,[52] this was an unexpected observation.

As denoted by the dotted arrows in Fig. 5(d), we found that the defects always appeared surrounded by a ring-shaped depression. These look quite similar to the Type-1 defect assigned to an oxygen atom in the as-grown film in Figs. 2(d) and 2(f).

To assign the chemical species in Figs. 5(a)–5(c), we obtained Ni 2p and O 1s core-level XPS spectra from the sur-
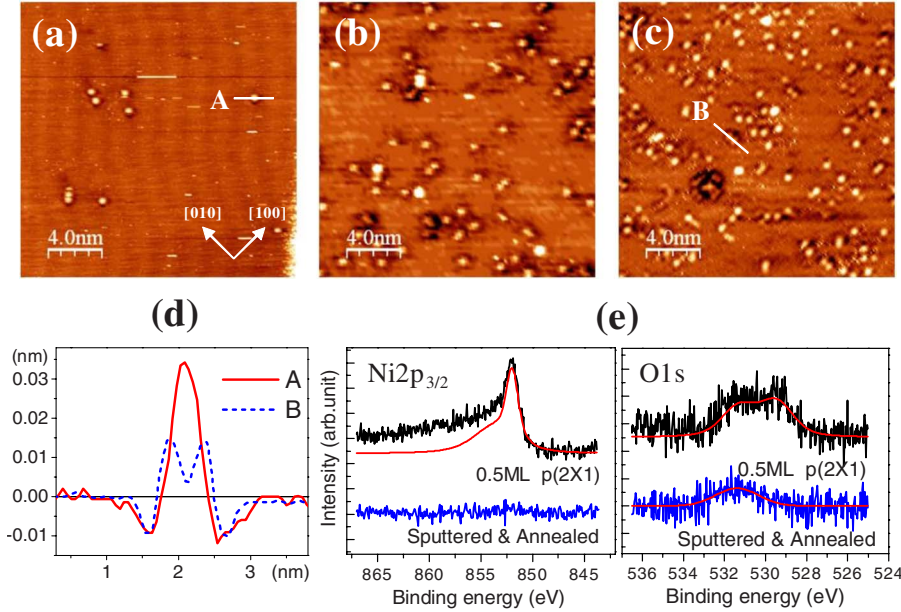
(a) A   [010] [100]   4.0nm

(b) 4.0nm

(c) B   4.0nm

(d)

(nm) 0.03 0.02 0.01 0.00 -0.01   A   B   1 2 3 (nm)

(e)

Ni2$p_{3/2}$ Intensity (arb.unit)   0.5ML p(2X1)   Sputtered & Annealed   865 860 855 850 845   Binding energy (eV)

O1s 0.5ML p(2X1)   Sputtered & Annealed   536 534 532 530 528 526 524   Binding energy (eV)

FIG. 5. (Color online) STM images obtained on the surfaces of 0.5 ML film after being sputtered and annealed at (a) 450, (b) 500, and (c) 550 °C. The STM images were taken with V_{sample}=0.2 V and I_{set}=0.5 nA. (d) Height profiles of particles along the lines A and B. The blue (dark gray) curves in (e) are Ni 2$p_{3/2}$ (left) and O 1s (right) core level XPS spectra of 0.5 ML film after being sputtered and annealed at 500 °C. The red (gray) curves, superimposed on the raw data, are the best fits for the experimental spectra after the Shirley-type background subtraction.

face shown in Fig. 5(b). These spectra are drawn as blue (lower) curves in Fig. 5(e). For comparison, spectra of the 0.5 ML film showing $p(2 \times 1)$ reconstruction are also presented as black (upper) curves.[53] Note that no Ni signal was observed after sputtering the film, while the oxygen signal was still clearly observed. This indicates that the ball-shaped defects observed in the STM images in Figs. 5(a)–5(c) were the oxygen atoms.

The integrated intensity of O 1s spectrum from the sputtered and annealed sample was approximately 20% of that obtained from the 0.5 ML $p(2 \times 1)$ NiO film.[22,54] Note that the 0.5 ML $p(2 \times 1)$ NiO layer on Ag(001) has about 2400 oxygen atoms in a 20×20 nm^2 region, the same area as the STM images in Fig. 5. Therefore, from the integrated intensity of the O 1s spectrum, we expect to observe ~480 oxygen atoms in Fig. 5(b) if they reside on or in the Ag surface layer. However, we could observe only 60–70 oxygen atoms in the STM image.

The probing depth of STM in most materials is 0.2–0.3 nm, that is about one unit-cell deep.[55] However, XPS taken with Mg Kα line can probe O as deep as 2.1 nm, as estimated by the inelastic mean free path of O 1s photoelectron.[56] Therefore, our observation indicates that much more oxygen atoms reside below the range that STM can measure.

Silver is not thermodynamically driven to be oxidized by molecular oxygen at temperatures below 350 °C and P_{O2} below 10 Torr. Further, even at P_{O2} of 1 atm, no evidence of silver oxidation has been found at RT.[57–59] In the case of thermal deposition, such as EBE, where the kinetic energy of the deposition species is only on the order of 0.1 eV, it is quite difficult for oxygen to enter the subsurface region. On the other hand, hyperthermal atomic oxygen can penetrate and form Ag$_2$O grains down to the depth of several μm in a Ag single crystal.[60] Oxygen projectile with kinetic energy higher than ~10 eV, which was formed by the laser ablation during PLD, should have penetrated into the deep region of the Ag substrate. Also, it is known that single crystalline Ag

can store atomic oxygen, and that annealing processes above 400 °C in UHV will cause the subsurface oxygen to easily diffuse to the surface region.[61–63] Figures 5(a)–5(c) confirm the outward diffusion of the oxygen atoms to the near-surface region by the sputtering and the annealing procedures. Note that the subsurface oxygen should generate a highly inhomogeneous strain field at the surface, and that they might contribute to the reduced diffusivity of deposits on the surface.

IV. SUMMARY AND CONCLUSION

We performed both microscopic and spectroscopic studies on submonolayers of nickel oxide grown by PLD, on Ag(001). We found that the nickel oxide film grew in a quasi-two-dimensional fashion. Below 0.5 ML coverage, the film growth proceeded via the nucleation stage, namely, by increasing the island density rather than the island size. After this extended nucleation stage, i.e., above 0.5 ML, the island coalescence played a major role in the nickel oxide film growth.

By combining STM with XPS, we could clearly identify numerous near-surface defects such as metallic Ni clusters embedded in the Ag substrate and oxygen atoms adsorbed on Ag(001). We also found that the embedded Ni clusters played the role of nucleation sites for nickel oxide islands. In addition, hyperthermal oxygen atoms produced by laser ablation during PLD caused subsurface oxygen defects.

Although it is very easy to deposit oxide thin films on soft metallic substrates, such as silver, by PLD, our work suggests that such film growth method requires precautions. The hyperthermal species in the laser plume can generate a high density of defects that will alter the growth mode of oxides and the physical properties of the interface from the ideal abrupt interface. There is still considerable room for improvement in PLD growth through the optimization of various growth parameters, such as laser intensity and duration.

*parksh1@snu.ac.kr

†jskim@sookmyung.ac.kr

[1] S. A. Chambers, Surf. Sci. Rep. **39**, 105 (2000).

[2] R. Franchy, Surf. Sci. Rep. **38**, 195 (2000).

[3] C.-G. Duan, S. S. Jaswal, and E. Y. Tsymbal, Phys. Rev. Lett. **97**, 047201 (2006).

[4] J. S. Moodera, L. R. Kinder, T. M. Wong, and R. Meservey, Phys. Rev. Lett. **74**, 3273 (1995).

[5] E. Y. Tsymbal and H. Kohlstedt, Science **313**, 181 (2006).

[6] J. Nogués and I. K. Schüller, J. Magn. Magn. Mater. **192**, 203 (1999).

[7] J. M. De Teresa, A. Barthélémy, A. Fert, J. P. Contour, F. Montaigne, and P. Seneor, Science **286**, 507 (1999).

[8] C. Heiliger, P. Zahn, B. Y. Yavorsky, and I. Mertig, Phys. Rev. B **72**, 180406(R) (2005).

[9] P. G. Mather, J. C. Read, and R. A. Buhrman, Phys. Rev. B **73**, 205412 (2006).

[10] W. H. Butler, X. G. Zhang, T. C. Schulthess, and J. M. MacLaren, Phys. Rev. B **63**, 054416 (2001).

[11] J. Shen and J. Kirschner, Surf. Sci. **500**, 300 (2002).

[12] D. A. Müller, N. Nakagawa, A. Ohtomo, J. L. Grazul, and H. Y. Hwang, Nature (London) **430**, 657 (2004).

[13] S. Seo *et al.*, Appl. Phys. Lett. **85**, 5655 (2004).

[14] C. B. Lee *et al.*, Appl. Phys. Lett. **91**, 082104 (2007).

[15] S. H. Phark, R. Jung, Y. J. Chang, T. W. Noh, and D. W. Kim, Appl. Phys. Lett. **94**, 022906 (2009).

[16] H.-J. Freund, H. Kuhlenbeck, and V. Staemmler, Rep. Prog. Phys. **59**, 283 (1996).

[17] M. Bäumer and H.-J. Freund, Prog. Surf. Sci. **61**, 127 (1999).

[18] H. D. Chopra, B. J. Hockey, P. J. Chen, W. F. Egelhoff, M. Wuttig, and S. Z. Hua, Phys. Rev. B **55**, 8390 (1997).

[19] K. Marre and H. Neddermeyer, Surf. Sci. **287-288**, 995 (1993).

[20] K. Marre, H. Neddermeyer, A. Chasse, and P. Rennert, Surf. Sci. **357-358**, 233 (1996).

[21] F. Müller, R. de Masi, P. Steiner, D. Reinicke, M. Stadtfeld, and S. Hüfner, Surf. Sci. **459**, 161 (2000).

[22] T. Bertrams and H. Neddermeyer, J. Vac. Sci. Technol. B **14**, 1141 (1996).

[23] I. Sebastian, T. Bertrams, K. Meinel, and H. Neddermeyer, Faraday Discuss. **114**, 129 (1999).

[24] J. Wollschläger, D. Erdös, H. Goldbach, R. Höpken, and K. M. Schröder, Thin Solid Films **400**, 1 (2001).

[25] C. Giovanardi, A. di Bona, S. Altieri, P. Luches, M. Liberati, F. Rossi, and S. Valeri, Thin Solid Films **428**, 195 (2003).

[26] P. Luches *et al.*, Thin Solid Films **400**, 139 (2001).

[27] B. Degroote, A. Vantomme, H. Pattyn, and K. Vanormelingen, Phys. Rev. B **65**, 195401 (2002).

[28] S. H. Phark, Y. J. Chang, T. W. Noh, and J.-S. Kim (unpublished).

[29] D. B. Chrisey and G. K. Hubler, *Pulsed Laser Deposition of Thin Films* (John Wiley & Sons, New York, 1994).

[30] T. Nakayama, Surf. Sci. **133**, 101 (1983).

[31] L. Wiedeman, H. S. Kim, and H. Helvajian, *MRS Symposia Proceedings*, Vol. 201 (Materials Research Society, Pittsburgh, 1991), p. 575.

[32] C. Girault, D. Damiani, J. Aubreton, and A. Catherinot, Appl. Phys. Lett. **55**, 182 (1989).

[33] H. Baker, *ASM Handbook* (ASM international, Materials Park, Ohio, 1992).

[34] K. S. Lee, S. H. Kim, H. G. Min, J. Seo, and J.-S. Kim, Surf. Sci. **377-379**, 918 (1997).

[35] M. Caffio, A. Atrei, U. Bardi, and G. Rovida, Surf. Sci. **588**, 135 (2005).

[36] D. A. Hite, O. Kizilkaya, P. T. Sprunger, M. M. Howard, C. A. V., Jr., H. Geisler, and D. M. Zehner, J. Vac. Sci. Technol. A **18**, 1950 (2000).

[37] S. L. Chang, J.-M. Wen, P. A. Thiel, S. Günther, J. A. Meyer, and R. J. Behm, Phys. Rev. B **53**, 13747 (1996).

[38] S. Schintke, S. Messerli, K. Morgenstern, J. Nieminen, and W.-D. Schneider, J. Chem. Phys. **114**, 4206 (2001).

[39] I. Costina, M. Schmid, H. Schiechl, M. Gajdos, A. Stierle, S. Kumaragurubaran, J. Hafner, H. Dosch, and P. Varga, Surf. Sci. **600**, 617 (2006).

[40] L. Vattuone, U. Burghaus, L. Savio, M. Rocca, G. Costantini, F. B. de Mongeot, C. Boragno, S. Rusponi, and U. Valbusa, J. Chem. Phys. **115**, 3346 (2001).

[41] Quantitative confirmation was done by the fractal analysis of the islands shown in Figs. 2(c) and 3(a). Complexity of an island boundary can be quantified by the exponent D of the equation $P = AS^{D/2}$, where P, S, D, and A are the perimeter length, area, fractal dimension, and proportion constant, respectively. As D decreases, the island boundary looks more straightened. The nickel oxide islands in the as-grown film of $\Theta = 0.5$ [shown in Fig. 2(c)] and those in the annealed one [shown in Fig. 3(a)] give $D = 1.75$ and 1.45, respectively.

[42] Note that there were theoretical predictions for the development of a surface state at ~ 0.6 eV above E_F (refer to 41, 42). However, our work, as well as earlier experimental work (refer to 23), could not confirm the existence of this predicted surface state.

[43] S. Casassa, A. M. Ferrari, M. Busso, and C. Pisani, J. Phys. Chem. B **106**, 12978 (2002).

[44] F. Cinquini, L. Giordano, G. Pacchioni, A. M. Ferrari, C. Pisani, and C. Roetti, Phys. Rev. B **74**, 165403 (2006).

[45] S. Schintke, S. Messerli, M. Pivetta, F. Patthey, L. Libioulle, M. Stengel, A. De Vita, and W.-D. Schneider, Phys. Rev. Lett. **87**, 276801 (2001).

[46] S. Großer, C. Hagendorf, H. Neddermeyer, and W. Widdra, Surf. Interface Anal. **40**, 1741 (2008).

[47] J. M. McKay and V. E. Henrich, Phys. Rev. B **32**, 6764 (1985).

[48] B. P. Payne, A. P. Grosvenor, M. C. Biesinger, B. A. Kobe, and N. S. McIntyre, Surf. Interface Anal. **39**, 582 (2007).

[49] A. Agrawal, H. R. Habibi, R. K. Agrawal, J. P. Cronin, D. M. Roberts, R. Caron-Popowich, and C. M. Lampert, Thin Solid Films **221**, 239 (1992).

[50] A. Davidson, J. F. Tempere, M. Che, H. Roulet, and G. Dufour, J. Phys. Chem. **100**, 4919 (1996).

[51] The current density of Ar^+ ions in our sputtering system is 61 $\mu A/cm^2$ at the sample surface. With the same condition, 30 min of sputtering was sufficient to remove 1.5 ML NiO film grown on single crystal Ag(001) by EBE. For the total sputtering time, i.e., 5 hours, the Ar ion fluence was about 7×10^4 nm^{-2}. The ion fluence at the sample surface is defined as (ion flux) × (time). Since the sputter yield of Ag is ~5.5 atoms per Ar^+ ion (refer to 49), the thickness of Ag(001) single crystal, removed by the sputtering, was estimated to be ~6.5 μm.

[52] N. Matsunami, Y. Yamamura, Y. Itikawa, N. Itoh, Y. Kazumata, S. Miyagawa, K. Morita, R. Shimizu, and H. Tawara, *Atomic Data and Nuclear Data* (Academic, New York, 1984).

[53] The spectra denoted by the black curves are those from the 0.5 ML nickel oxide film grown by EBE, which showed the well-known $p(2 \times 1)$ reconstructed structure. Since the $p(2 \times 1)$ reconstructed structure retains the 1:1 stoichiometry of Ni and O, the spectral intensity of the sputtered and annealed surface relative to that of $p(2 \times 1)$ structure can be used to estimate the amount of atomic species.

[54] C. Giovanardi, A. di Bona, and S. Valeri, Phys. Rev. B **69**, 075418 (2004).

[55] S. Heinze, R. Abt, S. Blügel, G. Gilarowski, and H. Niehus, Phys. Rev. Lett. **83**, 4808 (1999).

[56] S. Tanuma, C. J. Powell, and D. R. Penn, Surf. Interface Anal. **21**, 165 (1994).

[57] F. Besenbacher and J. K. Nøskov, Prog. Surf. Sci. **44**, 5 (1993).

[58] A. W. Czanderna, J. Phys. Chem. **68**, 2765 (1964).

[59] W.-X. Li, C. Stampfl, and M. Scheffler, Phys. Rev. Lett. **90**, 256102 (2003).

[60] L. Li, J. C. Yang, and T. K. Minton, J. Phys. Chem. C **111**, 6763 (2007).

[61] X. Bao, M. Muhler, B. Pettinger, R. Schlögl, and G. Ertl, Catal. Lett. **22**, 215 (1993).

[62] A. Boronin, S. Koscheev, O. Kalinkina, and G. Zhidomirov, React. Kinet. Catal. Lett. **63**, 291 (1998).

[63] B. Pettinger, X. Bao, I. Wilcock, M. Muhler, R. Schlögl, and G. Ertl, Angew. Chem. Int. Ed. Engl. **33**, 85 (1994).